J. Micromech. Microeng. **22** (2012) 065028 (7pp) doi:10.1088/0960-1317/22/6/065028

Control of buckling in large micromembranes using engineered support structures

Eiji Iwase[1,2,4], Pui-Chuen Hui[1], David Woolf[1], Alejandro W Rodriguez[1,3], Steven G Johnson[3], Federico Capasso[1] and Marko Lončar[1,4]

[1] School of Engineering and Applied Sciences, Harvard University, Cambridge, MA 02138, USA
[2] Department of Applied Mechanics and Aerospace Engineering, Waseda University, Tokyo 169-8555, Japan
[3] Department of Mathematics, Massachusetts Institute of Technology, Cambridge, MA 02139, USA

E-mail: iwase@waseda.jp and loncar@seas.harvard.edu

Received 24 January 2012, in final form 11 April 2012
Published 25 May 2012
Online at stacks.iop.org/JMM/22/065028

Abstract
In this paper we describe a general method to avoid stress-induced buckling of thin and large freestanding membranes. We show that using properly designed supports, in the form of microbeams, we can reduce the out-of-plane deflection of the membrane while maintaining its stiffness. As a proof of principle, we used a silicon-on-insulator (SOI) platform to fabricate 30 μm wide, 220 nm thick, free-standing Si membranes, supported by four 15 μm long and 3 μm wide microbeams. Using our approach, we are able to achieve an out-of-plane deformation of the membrane smaller than 50 nm in spite of 39 MPa of compressive internal stress. Our method is general, and can be applied to different material systems with compressive or tensile internal stress.

(Some figures may appear in colour only in the online journal)

1. Introduction

Freestanding micro membrane/beam structures are commonly used in microelectromechanical systems (MEMS) to realize variable capacitors [1], RF switches [1, 2], pressure sensors [3], mechanical memories [4] and movable mirrors [5]. In such freestanding structures, deformation by residual internal stress is a well known and common issue [6–8]. The stress, caused by the thermal expansion coefficient mismatch between different materials, is often built-in during the process of thin film deposition and is therefore difficult to avoid. This is a problematic since large compressive or tensile stresses can lead to buckling or breaking of the membrane. The degree of buckling depends on the length/thickness ratio of a membrane structure: if the ratio is 100 or larger, buckling can be significant even for low values of compressive stress (on the order of several tens of MPa). To reduce the effect of the internal stress, several stress-reduction techniques have been proposed, including optimization of the deposition conditions [9], postdeposition annealing [10], stress-compensation by a deposition of another film [5] and ion implantation [10, 11]. All of these stress compensation techniques, however, suffer two major drawbacks. First, they are material specific. Second, they only work in a narrow temperature range due to thermal expansion coefficients. In this paper, we describe a general method to control the out-of-plane strain and stiffness of suspended membranes by using properly designed supporting beam structures. We use this method to realize large, free-standing Si membranes perforated with a lattice of holes to define the photonic crystal (PhC) structure shown in figure 1.

Recently, there has been increasing interest in realizing PhC membranes that support guided resonances for applications in the field of optomechanics [12–18]. These membranes are typically fabricated in semiconductor materials exhibiting large dielectric permittivities, e.g. Si or InGaAs.

[4] Author to whom any correspondence should be addressed.

 © 2012 IOP Publishing Ltd Printed in the UK & the USA

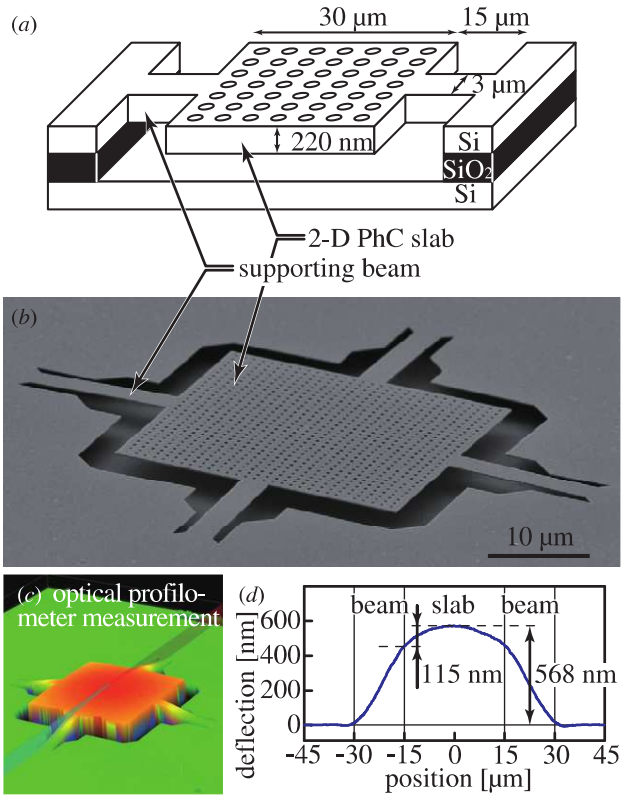

Figure 1. (*a*) Schematic image of a target structure with the typical lengths indicated. The structure consists of a thin and large 2D PhC slab supported by four beams. (*b*) SEM image of the structure. (*c*), (*d*) Built-in internal stress causes buckling of the photonic crystal membrane.

To ensure strong optomechanical interaction, thin (∼200 nm) and large (∼several tens of μm) membrane structures, with length/thickness ratios ∼100, are desired. The small thickness allows for greater flexibility of the membrane (to enable strong response of the structure to the weak forces), and ensure single-mode (optical) operation in the perpendicular direction, while the large area is needed to ensure good confinement of guided resonances supported by the PhC membrane. Furthermore, structures have been realized with membrane–substrate separations as small as a few hundred nanometers [13, 15–17] in order to enhance the optomechanical coupling. For all of these reasons, and to avoid the failure of the structure, it is essential to reduce buckling of the membrane due to built-in internal stress.

2. Design

A 2D PhC slab structure that supports guided resonances is shown in figure 1(*a*). It consists of a 220 nm thick free-standing Si square membrane of width 30 μm, supported by four microbeams of length 15 μm. The membrane is perforated with a PhC lattice of holes with periodicity $a = 1$ μm and hole radius $r = 200$ nm. The structure was realized in a commercial SOI wafer (SOITEC Inc.) with 220 nm thick Si device layer and 2 μm thick buried oxide (BOX) layer. The structure was fabricated using electron beam lithography followed by inductive coupled plasma reactive ion etching (ICP RIE) and HF vapor etching (figure 1(*b*)). As shown in the optical profilometer measurement in figures 1(*c*) and (*d*), the 2D PhC slab structure with simple straight supporting beams is buckled upward by its own internal stress.

In the case of a simple beam structure with length l, width w and thickness t, a critical buckling stress σ_c is proportional to $(t/l)^2$. In the case of doubly clamped beams, the critical buckling stress is given by $\sigma_c = \frac{\pi^2}{3}E\left(\frac{t}{l}\right)^2$, where E is the Young's modulus of the structure [19]. (Note: We describe a compressive stress as positive and a tensile stress as negative in this paper.) If the structure has a compressive internal stress σ_0 which is larger than the critical buckling stress ($\sigma_0 \geqslant \sigma_c$), then we can define a critical buckling length $l_c = \pi t\sqrt{\frac{E}{3\sigma_0}}$ so that all the beams with length $l > l_c$ will be buckled. A critical buckling length l_c of our SOI wafer for a $t = 200$ nm thick device layer can be estimated to be in the range of $l_c =$ 13–41 μm, given the internal stress in a typical commercial SOI wafer of $\sigma_0 = 10$–100 MPa and the Young's modulus $E = 169$ GPa for Si in the $\langle 1\,1\,0\rangle$ direction [20]. Therefore, buckling can be large even in a structure that is only a few tens of μm in length (figure 2(*a*)). We note that the critical buckling length increases to $l_c = 196$–620 μm if the thickness of the Si device layer is increased to $t = 3$ μm. To evaluate the built-in stress in the wafers used in this experiment, we fabricated arrays of doubly clamped beams with varying length and measured their out-of-plane deflection using a 3D optical profilometer (Olympus LEXT OLS4000, display resolution: 1 nm). The results, shown in figure 2(*b*), are in good agreement with the theoretical model discussed above. Using these values, we estimated the compressive internal stress of the Si device layer of the SOI to be 39 MPa, resulting in the critical buckling length $l_c = 26.3$ μm. This explains the significant buckling of the PhC membrane (figure 1), whose total length is larger than l_c.

In order to overcome this buckling issue, it is necessary to redesign the supporting beams. Fundamentally, buckling appears when a compressive internal stress acts as an axial load to a supporting beam (figure 3(*a*)). Therefore, our design methods are classified into three categories based on the type of the deflection induced by the compressive stress. The 'type 1' method (figure 3(*b*)), leads to in-plane buckling instead of out-of-plane buckling due to axial load by means of the compressive internal stress. The 'type 2' method (figure 3(*c*)), leads to in-plane deformation without buckling due to axial load by taking advantage of beams with an initial deflection (i.e. curved beams). The type 2 beams can be deformed below the in-plane critical buckling stress, whereas type 1 beams are deformed only by stresses above the in-plane critical buckling stress. The 'type 3' method (figure 3(*d*)) uses a lateral beam to transform the compressive stress into a lateral load. All approaches can be described as methods of releasing the internal stress by in-plane deformation.

For the type 1 method to work, it is necessary for the in-plane critical buckling stress $\frac{\pi^2}{3}E\left(\frac{w}{l}\right)^2$ to be smaller than the out-of-plane critical buckling stress $\frac{\pi^2}{3}E\left(\frac{t}{l}\right)^2$. Therefore, an extremely narrow and long beam is required which may be challenging to implement. In addition, type 1 is only effective

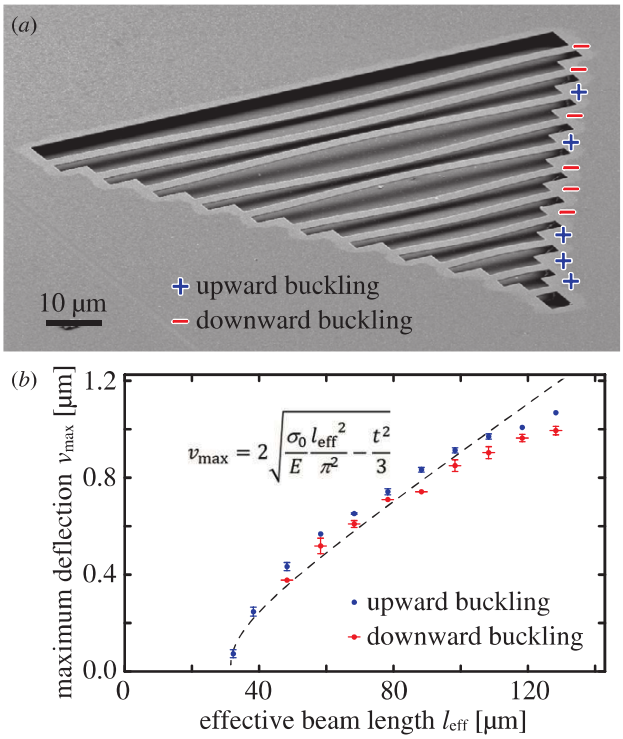

Figure 2. Characterization of stress-induced deformation in a commercial SOI wafer with $t = 220$ nm thick device layer. (*a*) The doubly clamped beams with different lengths are buckled upward or downward due to the internal stress. (*b*) Deflection of each beam as a function of its length. Eleven beams with lengths $l = 4$, 10, 20, 30, 40, 50, 60, 70, 80, 90, 100 μm have been evaluated. The horizontal axis is the effective beam length l_{eff} which is the sum of the designed beam length l and a constant undercut length. We estimate the undercut length to be 23 μm. Blue and red dots are deflections of upward and downward buckling, respectively. Error bars refer to the standard deviations of the deflection measurement. The slight difference between the amount of upward and downward buckling can be attributed to the stress gradient and bending moment at the ends. The dashed line is a fitting curve of a theoretical deflection $v_{max} = 2\sqrt{\frac{\sigma_0}{E}\frac{l_{eff}^2}{\pi^2} - \frac{t^2}{3}}$ [5] with σ_0.of 39 MPa.

in the case of compressive stress, while types 2 and 3 can be used for both compressive and tensile stress.

Types 2 and 3 are based a similar idea: the stiffness of a simple straight beam against an axial load (i.e. in-plane stiffness) is $E\frac{wt}{l}$. Therefore, if part of the beam has in-plane stiffness smaller than $E\frac{wt}{l}$, it can relieve the internal stress by elastic deformation. However, we do not want to reduce the out-of-plane stiffness (i.e. out-of-plane spring constant), because the supporting beams have to play two roles: (1) reducing the out-of-plane deformation and (2) supporting the membrane structure. Therefore we use a multiple-narrow-beam structure, shown in figure 4. Figure 4 shows the in-plane and out-of-plane stiffness of a simple straight beam and type 3 beams. Using a multiple-narrow-beam structure it is possible to reduce the in-plane stiffness while maintaining the out-of-plane stiffness of a simple straight beam. That is, if we change from a simple lateral beam to n beams each with a fraction $1/n$ of the original width, we obtain $1/n^2$ times smaller stiffness in

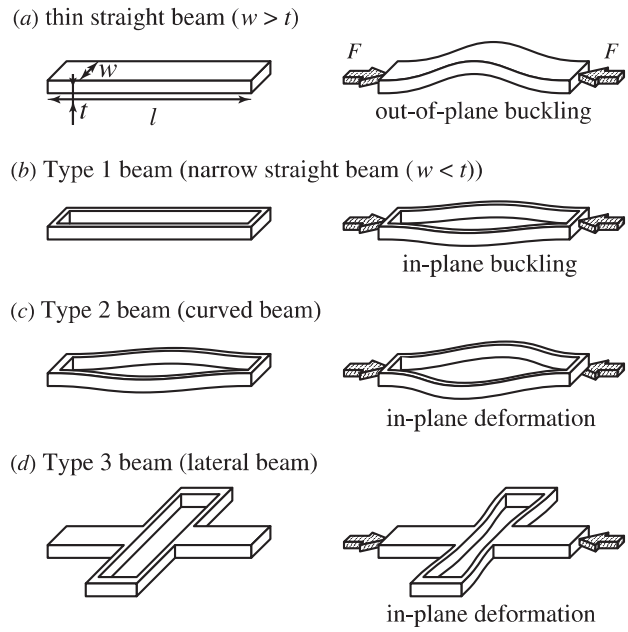

Figure 3. Different beam structures that can be used to overcome out-of-plane buckling due to an axial load. All approaches are based on inducing in-plane deformation to overcome the out-of-plane deformation due to an axial load.

the in-plane direction while maintaining the same out-of-plane stiffness (shown in figure 4). The same analysis applies to type 2 beams, and is shown in figure 5.

3. Fabrication and evaluation

To verify our designs, we fabricated the structures discussed in the previous section, using the same SOI wafer as in figure 2. The SEM images and the beam deflections measured using a 3D optical profilometer are shown in figure 6. The beams have length 100 μm, width 3 μm, and thickness 220 nm. Figure 6(*c*) shows a simple straight beam with 1212 nm of out-of-plane deflection due to buckling. Figure 6(*e*) shows a multiple-narrow-beam type 2 structure that consists of 8 narrow curved beams with 200 nm widths. Figure 6(*f*) shows a multiple-narrow-beam type 3 structure that consists of 15 narrow lateral beams with 200 nm widths. The maximum out-of-plane deflections of the multiple-narrow-beam types 2 and 3 structures are 280 nm and 114 nm, respectively. As can be seen, the out-of-plane deflections are highly reduced using our proposed methods. Figure 6(*d*) is a beam with multiple-narrow straight beams without initial deflection, so the beam also suffers out-of-plane buckling of 1211 nm. Though we could not measure the in-plane deformation in figure 6(*e*), we can obviously confirm the effect of initial deflection (i.e. curved beam) by comparing to the out-of-plane deflection of figure 6(*d*).

Figures 1(*b*) and 7(*a*), (*b*) show the photonic crystal membrane structures with simple, types 2 and 3 supporting beams, respectively. Using the profilometer, we measured the maximum upward deflections of types 2 and 3 to be 49 and 33 nm, respectively. This is more than an order of magnitude

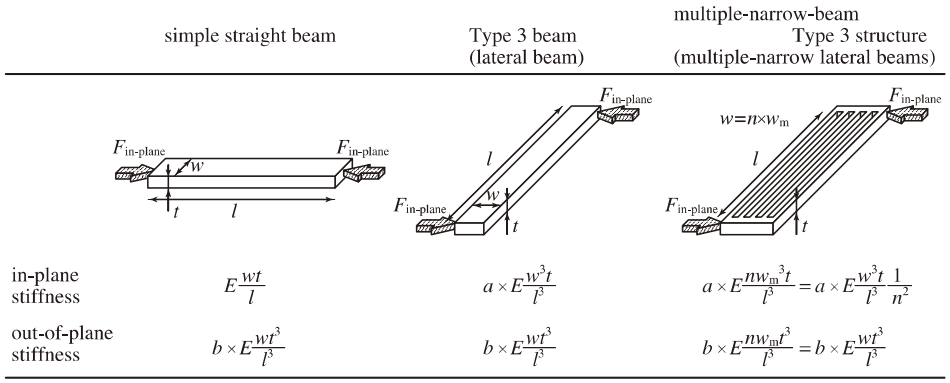

Figure 4. In-plane and out-of-plane stiffness of a simple straight beam and type 3 beams. Stiffness is defined by a load/deformation ratio (i.e. $F/v_{\max}$). In the case of a simple straight beam, the in-plane stiffness (for the axial load) is $E\frac{wt}{l}$ and the out-of-plane stiffness is proportional to $E\frac{wt^3}{l^3}$. The coefficients a and b are determined by load and end conditions. For example, in the case of a doubly clamped beam under point loading at the center, $a = b = 16$. In the case of a guided-clamped beam under point loading at the free end, $a = b = 1$ [21].

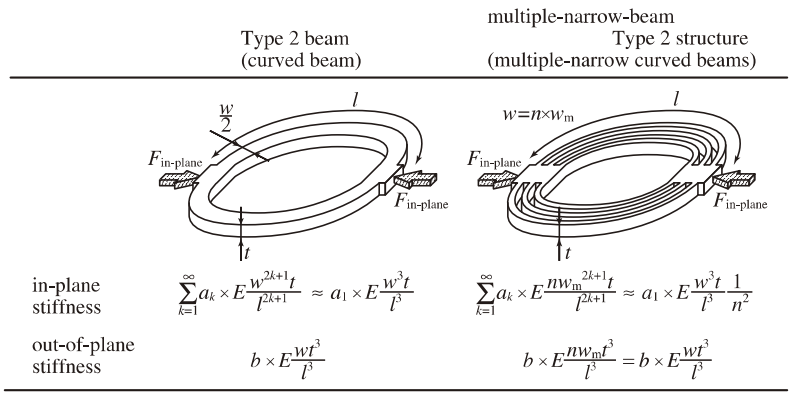

Figure 5. In-plane and out-of-plane stiffness of type 2 beams. We can use the same analysis as with type 3 under the assumption that the length/width ratio is large.

smaller than a maximum deflection (568 nm) measured for the membrane with simple supporting beams (figure 1(*b*)). Finally, we note that since the supporting beams relieve the internal stress, the membrane itself does not bend (up to the resolution of our apparatus) under its internal stress, and is very flat. This is of great importance for many photonic applications, including movable mirrors and variable capacitors.

4. Discussion

Approaches to reduce the out-of-plane buckling/deflection by designing proper supports, using methods that fall in to type 2 [22] or type 3 [23, 24] categories, have previously been studied. The novel aspect of our work is the application of multiple-narrow-beam structures that offer very important advantages over other methods: the in-plane and out-of-plane stiffness can be designed almost independently. That is, by increasing n, we can reduce the in-plane stiffness of the beam without changing the out-of-plane stiffness, and thus not change the spring constant of the membrane. This is important to designs of related devices such as variable capacitors, RF switches and movable mirrors.

In the case of a simple beam, the internal stress before (σ_0) and after (σ_{f}) releasing are the same, up to the critical buckling stress σ_{c} in compression or the breaking stress σ_{b} in tension (figure 8). Therefore the simple beam can be used as long as the internal stress σ_0 satisfies $\sigma_{\text{b}} < \sigma_0 < \sigma_{\text{c}}$. In the case of type 2 or type 3 beams, with smaller in-plane stiffness, σ_0 and σ_{f} are different due to the in-plane elastic deformation of the beam. Therefore, we define two new parameters, the highest allowable compressive stress σ_{AC} and the highest allowable tensile stress σ_{AT}, in the following way: if the initial stress σ_0 is σ_{AC} or σ_{AT}, the final stress σ_{f} would be σ_{c} or σ_{b}, respectively (see figure 8). As a result, types 2 and 3 beams can be used as long as the initial internal stress σ_0 satisfies $\sigma_{\text{AT}} < \sigma_0 < \sigma_{\text{AC}}$. In the case of the multiple-narrow-beam structure, σ_{AC} and σ_{AT} are proportional to n^2. Therefore it is always possible to choose n satisfying this condition, which makes our approach general and useful for a range of geometries and films deposited using different techniques. However, in practice the upper limit of n is set by the minimum resolution of the fabrication process; the larger the n, the smaller the width of each beam in the multibeam section. If the characteristic beam width is w_0 and the minimum available width on the fabrication is $w_{\min}$, n should be smaller

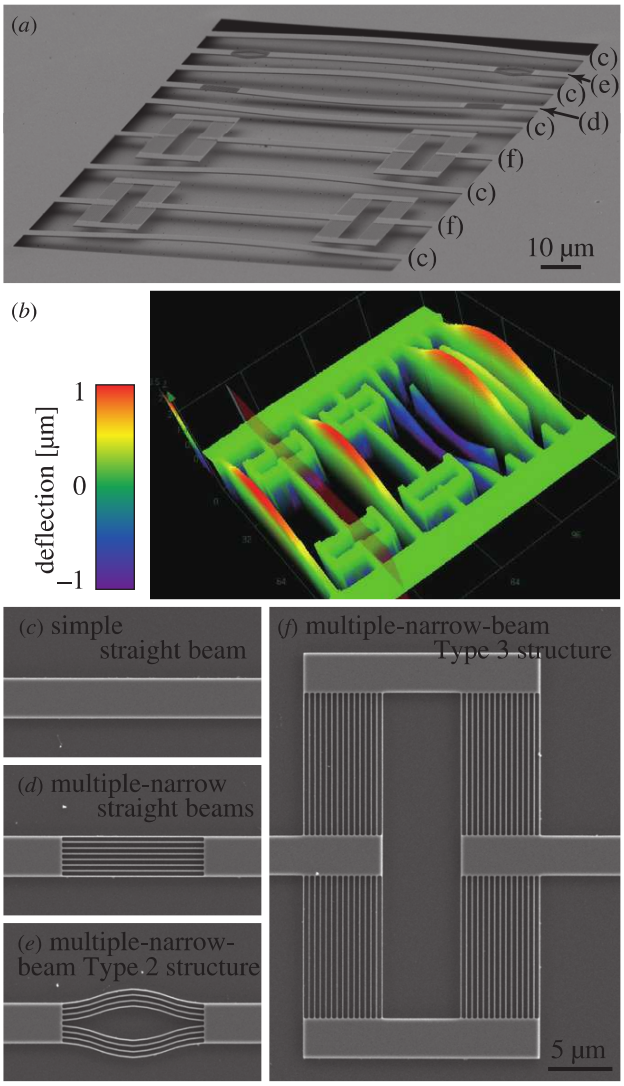

(g)

	(c)	(d)	(e)	(f)
maximum deflection	1,212 nm	1,211 nm	280 nm	114 nm

Figure 6. Doubly clamped beams with different support beam structures. All beams are 100 μm long and 3 μm wide. (*a*) SEM image of the beams. Note that the labels in this figure correspond to the SEM images below. (*b*) Measurement of the deflections obtained using a 3D optical profilometer. (*c*)–(*f*) Enlarged images of each beam structure before releasing. (*g*) Table showing the maximum deflection of the beams.

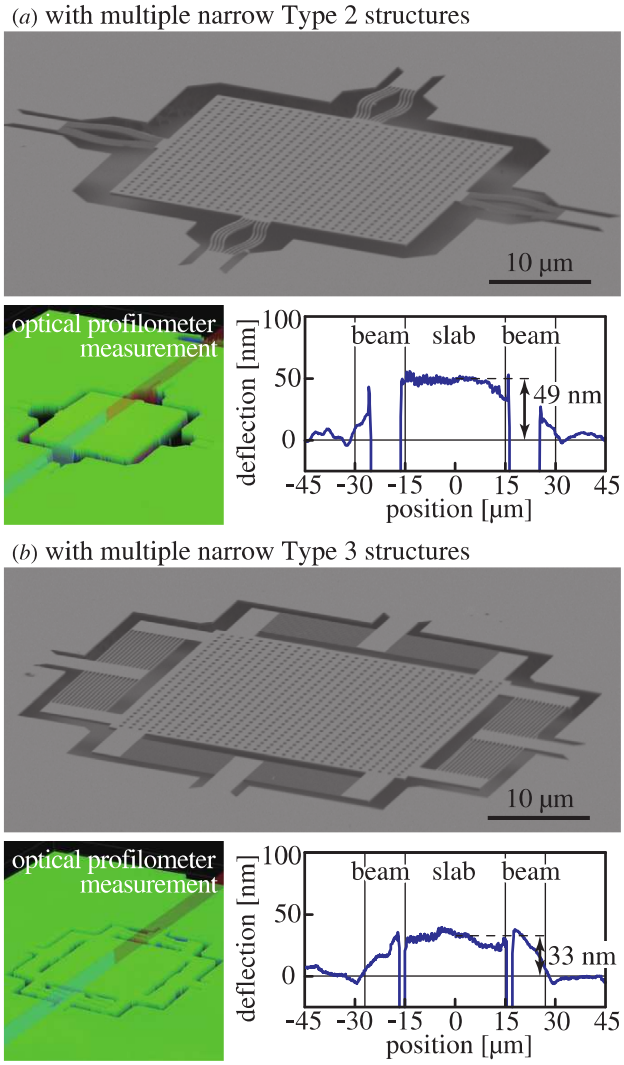

Figure 7. 2D PhC slab structures with supporting beams. The period and hole radius of the PhC slab is 1 μm and 200 nm, respectively. The dimension of the slab is 30 μm by 30 μm, and characteristic length and width of the supporting beams are 15 μm and 3 μm, respectively. (*a*) and (*b*) are structures with multiple-narrow-beam type 2 and 3 structures, respectively. Structure with simple beams, fabricated on the same wafer, is shown in figure 1(*b*). The 'noise' in the measurement at the position of the slab is due to the photonic crystal holes with sizes below the resolution limit of the profilometer.

than $w_0/w_{\min}$. For example our characteristic beam width was 3 μm and the minimum resolution is approximately 50 nm, because of our use of electron beam lithography, the upper limit of n is 60. As mentioned above, the allowable stresses σ_{AC} and σ_{AT} are proportional to n^2, so our method in this geometry can be used to deal with a wide range of internal stress. This is another unique feature of our method that has not been previously investigated. Our approach is material-platform nonspecific which further adds to its versatility. In addition, because our method can release internal stress of any magnitude as long as the stress is smaller than the allowable internal stresses, we do not have to know the precise internal stress of the membrane. In other words, if we choose a large enough value n, our beams make proper in-plane deformations according to the magnitude of internal stress automatically. This is very effective, especially for mitigating of temperature-induced stress whose value can greatly vary with temperature: our approach's 'self-adaptability' to internal stress makes it effective for a wide range of temperatures.

Though our method highly reduces the out-of-plan deflection, the structures still have finite deflection <50 nm. We believe that this is due to the stress gradient of the

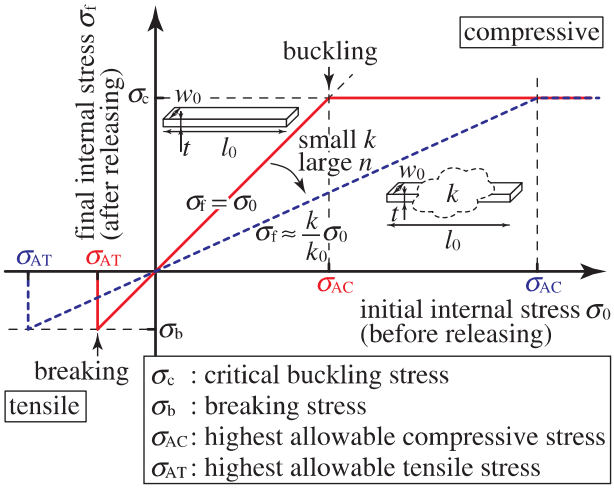

Figure 8. Illustration of the proposed stress-control approach based on engineered support structures. The released membrane structure is flat (no buckling) when the final internal stress after releasing (σ_f) is between σ_c and σ_b, where σ_c and σ_b are the critical buckling stress and the breaking stress, respectively. Corresponding to an initial internal stress before releasing σ_0, σ_0 should have a value between σ_{AC} and σ_{AT}, where σ_{AC} and σ_{AT} are the highest allowable compressive and tensile stress, respectively. The red and blue lines show the cases of a simple straight beam and a beam with a smaller stiffness region, respectively. In the case of a simple straight beam, σ_{AC} and σ_{AT} are the same as σ_c and σ_b, respectively (red line). But the beam has smaller stiffness beam with k in the in-plane stiffness, σ_{AC} and σ_{AT} is enlarged approximately as $\frac{k_0}{k}\sigma_c$ and $\frac{k_0}{k}\sigma_b$, where $k_0 = E\frac{w_0 t}{l_0}$, l_0 is the beam length from end to end, and w_0 is the beam width at the end (blue dashed line). If the multiple-narrow-beam type 2 or type 3 structure is used, the in-plane stiffness k is described by the formula $k = \frac{a}{n^2}E\frac{w^3 t}{l^3}$ (as shown in figures 4 and 5), where n is the number of nanobeams used in the structure.

membrane and/or a bending moment at its ends, which can also cause asymmetric upward and downward deflections. Indeed, it can be seen in figure 2(*b*) that the upward and downward deflections are slightly different (∼80 nm). The stress gradient comes from the wafer fabrication process and the bending moment at the ends comes from the residue of the sacrificial layer under the membrane. Since the 2D PhC slab region is very flat (in figures 7(*a*) and (*b*)) and most of the deflection occurs at the supporting beam region, we can conclude that the residual deflection is not due to the stress gradient, but rather due to the bending moment at the beam ends. Though our method cannot deal with a stress gradient or a bending moment at the ends, these effects cause little deflection in our demonstration.

5. Conclusions

We proposed a method to reduce the out-of-plane deflection of a membrane structure due to its internal stress, while maintaining the out-of-plane stiffness of the structure. Using the multiple-narrow-beam type 2 and 3 structures as supporting beams, it is possible to precisely engineer the residual stress simply by changing the number of beams (n). Applying our methods to a commercial SOI wafer with 39 MPa of compressive internal stress, we were able to reduce the out-of-plane deflection of the freestanding membrane by more than an order of magnitude, from 568 nm to below 50 nm. In the cases of type 2 and 3 structures, the maximum deflections were 49 and 33 nm, respectively. The characteristic length and thickness of the membrane structure is 60 μm and 220 nm, respectively, so that the length/thickness ratio of our membrane structure is 273 and the maximum deflection/length ratio is less than 1/1000. These values mean the freestanding thin and large membrane structure has little out-of-plane bending. In addition, our method can deal with a wide range of stress values and therefore is suitable for the compensation of not only the compressive but also the tensile internal stress. Furthermore, it can operate in a wide temperature range, since it can handle temperature-induced stress.

Acknowledgments

This work was supported by the Defense Advanced Research Projects Agency (DARPA) under contract no N66001-09-1-2070-DOD. The deflection measurement was performed by the 3D optical profilometer Olympus LEXT OLS4000 owned by Prof. Robert Wood at Harvard University. The microstructure fabrication was carried out using the facilities of Center for Nanoscale Systems (CNS) at Harvard University.

References

[1] Yao J J 2000 RF MEMS from a device perspective *J. Micromech. Microeng.* **10** R9–R38
[2] Rebeiz G M and Muldavin J B 2001 RF MEMS switches and switch circuits *IEEE Microw. Mag.* **2** 59–71
[3] Eaton W P and Smith J H 1997 Micromachined pressure sensors: review and recent developments *Smart Mater. Struct.* **6** 530–9
[4] Bagheri M, Poot M, Li M, Pernice W P H and Tang H X 2011 Dynamic manipulation of nanomechanical resonators in the high-amplitude regime and non-volatile mechanical memory operation *Nat. Nanotechnol.* **6** 726–32
[5] Min Y H and Kim Y K 1999 Modeling, design, fabrication and measurement of a single layer polysilicon micromirror with initial curvature compensation *Sensors Actuators* A **78** 8–17
[6] Fang W and Wickert J A 1994 Post buckling of micromachined beams *J. Micromech. Microeng.* **4** 116–22
[7] Fang W and Wickert J A 1996 Determining mean and gradient residual stresses in thin films using micromachined cantilevers *J. Micromech. Microeng.* **6** 301–9
[8] Creek S and Chitica N 1999 Deflection of surface-micromachined devices due to internal, homogeneous or gradient stresses *Sensors Actuators* A **78** 1–7
[9] Fu X A, Jezeski R, Zorman C A and Mehregany M 2004 Use of deposition pressure to control residual stress in polycrystalline SiC films *Appl. Phys. Lett.* **84** 341
[10] Camassel J and Tiberj A 2003 Strain effects in device processing of silicon-on-insulator materials *Appl. Surf. Sci.* **212** 742–8
[11] Bifano T G, Johnson H T, Bierden P and Mali R K 2002 Elimination of stress-induced curvature in thin-film structures *J. Microelectromech. Syst.* **11** 592–7
[12] Suh W, Yanik M F, Solgaard O and Fan S H 2003 Displacement-sensitive photonic crystal structures based on guided resonance in photonic crystal slabs *Appl. Phys. Lett.* **82** 1999–2001

[13] Notomi M, Taniyama H, Mitsugi S and Kuramochi E 2006 Optomechanical wavelength and energy conversion in high-Q double-layer cavities of photonic crystal slabs *Phys. Rev. Lett.* **97** 023903

[14] Kanamori Y, Kitani T and Hane K 2007 Control of guided resonance in a photonic crystal slab using microelectromechanical actuators *Appl. Phys. Lett.* **90** 031911

[15] Roh Y G, Tanabe T, Shinya A, Taniyama H, Kuramochi E, Matsuo S, Sato T and Notomi M 2010 Strong optomechanical interaction in a bilayer photonic crystal *Phys. Rev.* B **81** 121101

[16] Rodriguez A W, Woolf D, Hui P C, Iwase E, McCauley A P, Capasso F, Loncar M and Johnson S G 2011 Designing evanescent optical interactions to control the expression of Casimir forces in optomechanical structures *Appl. Phys. Lett.* **98** 194105

[17] Rodriguez A W, McCauley A P, Hui P C, Woolf D, Iwase E, Capasso F, Loncar M and Johnson S G 2011 Bonding, antibonding and tunable optical forces in asymmetric membranes *Opt. Express* **19** 2225–41

[18] Midolo L, van Veldhoven P J, Dundar M A, Notzel R and Fiore A 2011 Electromechanical wavelength tuning of double-membrane photonic crystal cavities *Appl. Phys. Lett.* **98** 211120

[19] Hibbeler R C *Mechanics of Materials* 8th edn (New Jersey: Prentice Hall) p 667

[20] Hopcroft M A, Nix W D and Kenny T W 2010 What is the Young's modulus of silicon? *J. Microelectromech. Syst.* **19** 229–38

[21] Young W C, Budynas R G and Dadegh A M *Roark's Formulas for Stress and Strain* 8th edn (New Jersey: McGraw-Hill) pp 208–9

[22] Elshurafa A M and El-Masry E I 2006 Finite-element modeling of low-stress suspension structures and applications in RF MEMS parallel-plate variable capacitors *IEEE Trans. Microw. Theory Tech.* **54** 2211–9

[23] Pisano A P and Cho Y H 1990 Mechanical design issues in laterally-driven microstructures *Sensors Actuators* A **23** 1060–4

[24] Young D J, Boser B E, Malba V and Bernhardt A F 2001 A micromachined RF low phase noise voltage-controlled oscillator for wireless communications *Int. J. RF Microw. Computer-Aided Eng.* **11** 285–300